Three-Dimensional Particle Simulations of NSTAR Ion Optics

Joseph Wang

Dept. Aerospace & Ocean Engineering, Virginia Polytechnic Institute and State University

James Polk, John Brophy, Ira Katz

Jet Propulsion Laboratory, California Institute of Technology

Abstract

A fully three-dimensional computer particle simulation model for ion optics is developed. This model allows multiple apertures to be included explicitly in the simulation domain and makes no assumptions on the upstream sheath. Simulation results are compared against grid erosion measurements obtained during the long duration test of the NSTAR ion thruster. It is shown that the simulation not only predicts accurately all features in the erosion pattern observed experimentally but also gives excellent quantitative agreement with measured erosion depth.

1. Introduction

Ion optics modeling is becoming an ever more important element in ion propulsion research and development activities. The nature of plasma flow in ion optics has rendered computer particle simulation, which solves plasma particle trajectory, space charge, and the Poisson's equation self-consistently, as the preferred modeling method. Some recent ion optics simulation studies can be found in Peng et al.[1994], Arakawa and Nakano[1996], Boyd et al.[1998], Nakano and Arakawa[1999], Tartz et al.[1999], Okawa and Takegahara [1999], Muravlev and Shagayda[1999], Nakayama and Wilbur [2001], etc (and references therein). The majority of ion optics models are axisymmetric models. The axisymmetric formulation does not take into account of the hexagonal layout of the ion optics aperture array. The currently available 3-dimensional ion optics models are all designed for a single grid aperture by considering the six-fold hexagonal symmetry of the aperture array, and simulations are performed for a cross section of one twelfth of a single aperture (30 degree by 60 degree right-triangle cross section). Due to computationally constraints, many ion optics models have further simplified the problem by using a pre-determined beam ion emission surface to represent the effects of the upstream presheath.

In this paper, we present a more generalized, fully 3-dimensional ion optics model. The code is designed in such a way that not only single aperture but also multiple apertures can be included explicitly in the simulation domain. Additionally, the model makes no assumptions on the upstream presheath and simulates ion beam extraction from the discharge plasma self-consistently.

The major challenge in applying the particle simulation method as a design tool is to build up a code that is sophisticated enough so the complex geometry associated with the optics can be modeled properly and yet computationally efficient enough so large-scale 3-dimensional particle simulations can be performed routinely within a reasonable time period. Complex geometries are usually best handled by tetrahedral cells or unstructured grids and finite-element based formulations. However, a tetrahedral cell based or unstructured grid based particle code can be significantly computationally more expensive than a standard orthogo-

nal grid PIC code. In a standard orthogonal grid PIC code, the location of memory of quantities defined in neighboring cells can be found trivially via indexing. This is in contrast to an unstructured grid where the neighbors of a given cell must be found by lookups in a table or other methods requiring additional memory references. Moreover, for either tetrahedral cells or unstructured grids, a fairly complex scheme is typically needed to determine a particle's new cell [Westermann, 1992]. These added complexities can make large-scale 3-D ion optics simulations prohibitively expensive because a particle code typically spends most of its computing time pushing particles and performing particle-grid interpolations [Wang et al.,1999].

Out of considerations for computational efficiency for large-scale simulations, the model presented here is build upon standard orthogonal grids and a finite-difference based formulation in electric field solve. To resolve the geometry associated with the optics apertures, a method of subgridscale placement of boundaries [Grote,1994] is used. This method explicitly includes the location of the optics wall in relation to the grid in the finite-difference form of Poisson's equation. We find that such an approach is sufficient for this particular problem and allows us to retain the computational efficiency associated with an orthogonal grid particle-in-cell (PIC) code.

This code is being applied to help the analysis of the results from the long duration test (LDT) of Deep Space 1 flight spare ion thruster[Polk et al, 1999]. This paper will also present a first comparison of grid erosion calculated using our particle simulation results against erosion measurements obtained during LDT.

2. Simulation Model

The ion optics model includes an ion beamlet simulation code and a charge exchange ion simulation code. In a simulation, the ion beamlet code is first used to simulate ion beam extraction from the discharge plasma. As the space charge from the charge exchange ions is negligible compared to that of the beam ions, the charge exchange ions have little effects on the beam ion trajectories, and are thus are not included in the ion beamlet simulation. Once a steady state for ion beamlets (from the upstream through the optics to downstream) has been achieved, the beam ions are frozen and we start simulations on charge-exchange ions. The ion beamlet density profile obtained by the beamlet code is used to calculate the volumetric charge-exchange ion production rate for every cell in the simulation domain, which is then used to generate charge-exchange ions in a simulation.

The simulation domain can be set up to include single as well as multiple apertures. Since we have only implemented symmetric boundary condition, currently the simulation boundaries can be taken on any of the "symmetric" surfaces. The "minimum" simulation cross section will be a cross section including two quarter-size holes. Note that this minimum cross section fully accounts for the geometric effects from a hexagon layout of the aperture arrays.

Along the acceleration direction (z direction), the upstream boundary represents the discharge chamber plasma, which has a plasma potential Φ_0, density n_0, and electron temperature T_{e0}. We make no assumptions about the upstream screen grid plasma sheath. The ion current extracted is determined self-consistently from the acceleration voltage and the upstream plasma boundary condition.

The downstream boundary represents the neutralized propellant plasma, which has a plasma potential Φ_∞, density n_∞, and electron temperature $T_{e\infty}$. We define a quasi-neutral zone near the downstream boundary within which we assume that the propellant ions are neutralized. We take the downstream plasma density to be the average ion density within the quasi-neutral zone. Hence, unlike other boundary parameters, the downstream density n_∞ is updated at every time step.

Similar to other ion optics codes, the ions are represented by macro-particles. A Boltzmann relationship between the electron density and local electrostatic potential is assumed for both the regions upstream of the screen grid and downstream of the acceleration grid. Specifically, the electron density in the region upstream of the screen grid is

given by

$$n_e = n_0 \exp(\frac{\Phi - \Phi_0}{T_{e0}}), \quad \Phi < \Phi_1 \tag{1}$$

$$n_e = n_0(1 + \frac{\Phi - \Phi_0}{T_{e0}}), \quad \Phi > \Phi_1 \tag{2}$$

and the electron density in the region downstream of the acceleration grid is given by

$$n_e = n_\infty \exp(\frac{\Phi - \Phi_\infty}{T_{e\infty}}), \quad \Phi < \Phi_\infty \tag{3}$$

$$n_e = n_\infty(1 + \frac{\Phi - \Phi_\infty}{T_{e\infty}}), \quad \Phi > \Phi_\infty \tag{4}$$

The electric field, space charge, and ion trajectories are solved self-consistently from the Poisson's equation

$$\bigtriangledown^2\Phi = -4\pi(n_i - n_e) \tag{5}$$

and the Newtown's second law

$$\frac{dm\vec{V}}{dt} = \vec{F} = q\vec{E}, \quad \frac{d\vec{x}}{dt} = \vec{V} \tag{6}$$

In ion beamlet simulations, the propellant ions are injected into the simulation domain from the upstream boundary. The upstream density and injection velocity are input variables. How much ion current can be extracted by the optics is a function of the upstream plasma condition. To perform ion beamlet simulations properly, one needs to accurately resolve the sheath upstream of the screen grid. In simulations, one needs to set the upstream boundary far enough from the screen grid and the cell size needs to be no larger than the Debye length based on the upstream plasma density. In order to have a stable solution for the upstream sheath, the ions are injected into the domain from upstream boundary with the Bohm velocity.

In charge-exchange ion simulations, the charge-exchange ions within the simulation domain are produced according to

$$\frac{dn_{cex}}{dt} = n_b(\vec{x})n_n(\vec{x})v_b\sigma_{cex} \tag{7}$$

The value of beam ion density n_b is determined in the ion beamlet simulation. The value of neutral density n_n is related to the beam current by the propellant utilization efficiency. The charge-exchange ion collision cross section is based on data presented in [Pullins et al., 2000]. To perform charge-exchange ion simulations properly, one needs to account for all the charge-exchange ions that will backflow. In order to do so, one should set the downstream boundary at a "sufficiently large" distance away from the accel grid to include the beam neutralization plane. One could estimate that such a distance is around the location where neighboring ion beamlets meet. Extracting from the results of ion beamlet simulation, we find that the neighbouring ion beamlets meet at a distance of about 2 cm downstream of the accelerator grid for the NSTAR ion thruster. However, the cell size used in the ion beamlet simulation is limited by the upstream plasma Debye length, which is on the order of 10^{-3}cm. Due to computationally constraints, we are unable to use such a large simulation domain. Hence, in charge-exchange ion simulations, one typically needs to inject a charge exchange ion current from the downstream boundary to represent those charge-exchange ions produced at a location beyond the simulation boundary.

As stated in the introduction, we decide to build our simulation code on orthogonal grids rather than more sophisticated grids, such as unstructured grids or tetrahedral cells, out of considerations for computational efficiency. To match the optics wall boundary, we adopt a method of subgridscale placement of boundaries, which explicitly includes the location of the optics wall in relation to the grid in the finite-difference form of Poisson's equation[Grote,1994]. This method can be easily illustrated with the finite-difference form of 1-D Poisson's equation:

$$\frac{\Phi_{i+1} - 2\Phi_i + \Phi_{i-1}}{h^2} = -\rho_i \tag{8}$$

Let's consider that the edge of a conductor surface is between grid points i and $i+1$, where grid point i is outside the conductor and grid point $i+1$ is inside the conductor. The distance between the conductor surface and grid point i is δ. We assume that the potential at the edge would be interpolated linearly

$$\Phi_{edge} = (1 - \delta)\Phi_i + \delta\Phi_{i+1} \tag{9}$$

Note that Φ_{edge} is the known surface potential of the conductor and Φ_{i+1} is a free parameter since it is inside the conductor. By substituting Φ_{i+1} in eq(8) with the above interpolation relation: $\Phi_{i+1} = (\Phi_{edge} - (1-\delta)\Phi_i)/\delta$, we obtain the finite difference equation at conductor surface

$$\frac{-(2+(1-\delta)/\delta)\Phi_i + \Phi_{i-1}}{h^2} = -\rho_i - \frac{\Phi_{edge}}{h^2} \quad (10)$$

Note that in the above equation, Φ_i approaches Φ_{edge} as $\delta \rightarrow 0$. This method extends easily to three dimensions. The linear interpolation is done independently in each direction for which there is a conducting object boundary.

To solve the nonlinear Poisson's equation in a 3-dimensional space, we have employed a dynamic alternating direction implicit (DADI) method [Doss et al.,1979; Hewett et al.,1992] with a defect correction using the Douglass-Gunn operator splitting [Douglas and Gunn,1964]. This DADI method was chosen over other algorithms for its increased stability properties over fully explicit methods and its relatively simple tridiagonal system of equations produced by the partially implicit nature of the method. This DADI based field solver is described in detail in [Wang et al., 2001].

3. Simulation Results

The results from a typical simulation are shown in Figures 1 to 4. This simulation is performed for nominal geometric and operating conditions of the NSTAR ion engine, listed in Table 1. The simulation domain includes 2 quarter-size apertures. The beam direction is along the z direction. The hole centers are located at $(x, y) = (0, 0)$ and $(x, y) = (1.1mm, 1.9mm)$.

The beam current extracted by the optics varies with the discharge plasma density far upstream of the screen grid. In this simulation, we consider a discharge plasma density of $n_0 = 2 \times 10^{11}\ cm^{-3}$. The upstream plasma potential and temperature are $\Phi_0 = 1100$V and $T_{e0} = 5$eV, and the downstream plasma potential and temperature are $\Phi_\infty = 0$V and $T_{e\infty} = 1.5$eV.

For the simulation presented here, the number of cells used are $30 \times 30 \times 204$. The cell sizes are $dy = 1.732dx$, $dx = dz$, where $dz = \lambda_{D0}$. For the given upstream plasma condition, $\lambda_{D0} = 3.7 \times 10^{-3}$cm. The total number of test particles used in the ion beamlet simulation is about 1.5 million particles and that in the charge exchange ion simulation is about 8.5 million. The upstream boundary is located at $30\lambda_{D0}$ from the screen grid. A series of test runs on the location of upstream boundary and cell size to ensure the simulation results do not depend on the numerical parameters used.

screen hole diameter d_s	1.91 mm
screen grid thickness t_s	0.38 mm
accel hole diameter d_a	1.14 mm
accel grid thickness t_a	0.51 mm
screen to accel grid gap g	0.58 mm
center-to-center hole spacing l	2.21 mm
total accelerating voltage	1100 V
screen grid voltage	1074 V
accel grid voltage	-180 V

Table 1: Nominal geometric and operating parameters for the NSTAR ion engine

Fig. 1 shows the 3-D potential contours on a z-x cutting plane, a z-y cutting plane, and several x-y cutting planes as well as the directions of beam ion velocity vectors. For the ion optics parameters listed in Table 1 and a discharge plasma with density $n_0 = 2 \times 10^{11}\ cm^{-3}$ and electron temperature $T_{e0} = 5$eV, the current extracted is $I_b \simeq 0.184$ mA/beamlet. The screen grid transparency is about 73%, and the accel grid transparency is 100%. Comparing the value of the extracted beam current in the simulation with the measured ion beamlet profile over the NSTAR grid, we find that this case corresponds to an aperture at about 5.8 cm radius.

Fig. 2 shows the directions of the charge-exchange ion velocity vectors. We plot separately for those charge-exchange ions originated within about 0.15 cm downstream of the accel grid (including those produced within the aperture) and

those originated at a location beyond 0.15 cm downstream of the accel grid. While the charge-exchange ions produced near the accel grid have a range of incident angles on the downstream face of the accel grid, those produced further downstream have almost normal incidence angles.

The total charge exchange ion current collected by the accel grid from the surface between the two quarter-size holes is about $I_{cex} \simeq 3.4 \times 10^{-4}$mA. Within that current, about 4×10^{-5}mA is from charge exchange ions originated within 0.15 cm of the accel grid. About 62% of the 4×10^{-5}mA is collected by the downstream face of the accel grid, and 38% is collected by the wall inside the aperture. On the other hand, all charge-exchange ions originated from beyond 0.15 cm downstream of the accel grid hit the downstream face. Hence, the erosion on the downstream face is primarily caused by charge exchange ions coming from far downstream.

Figs. 3 and 4 show the result of the charge-exchange ion impingement on the downstream surface of the accel grid. In Fig.3, we show impingement due to charge exchange ions produced within about 0.15cm of the accel grid, whereas in Fig.4, we show impingement due to charge exchange ions produced beyond a distance of 0.15cm downstream of the accel grid. In each figure, we show contours of impingement ion current density, ion number flux, ion energy distribution, and incident angle distribution. The results indicate that ions produced further downstream will produce a very different erosion pattern from the ions produced closer to the accel grid due to different focusing effects from the electric field.

4. Comparison Against Erosion Measurements

Based on the distribution of ion incident flux, energy, and angle over the accel grid surface, we can calculate grid erosion. Figs. 5 and 6 compares the calculated grid erosion against erosion measurement taken during the long duration test of the NSTAR ion thruster at JPL [Polk, 1999]. Simulation and measurement show an excellent agreement.

Fig. 5 examines erosion pattern on the downstream surface of the accel grid. In Fig. 5, the left pannel is a photograph of erosion and deposition pattern after 8200 hours of operation, the middle pannel shows erosion from simulation results for the same operating conditions, and the right pannel overlays the simulation result on the experimental data. A direct comparison shows that the simulation accurately predicts the erosion pattern. The simulation picks up all of the detailed features in the deposition pattern, including the little islands that occur around the hole at the azimuthal locations of the pits.

Fig. 6 compares erosion depth along and across the groove. For this case, the maximum eroded depth from simulation is about 208 microns, while the pit depth from the long duration test is 220-230 micron. The simulation also shows an excellent agreement with the measurement in the groove pattern. The net erosion on the plateau around the pits and grooves from simulation disagrees with the profilometer data. The reason that less erosion is observed in these locations is because carbon deposits protected the grid in these locations during the LDT. The simulation also gives excellent quantitative agreement with erosion measurements.

5. Summary and Conclusions

In summary, a fully three-dimensional particle simulation model for ion optics has been developed. Out of considerations for computational efficiency for large-scale simulations, this code is build upon standard orthogonal grids and a finite-difference based formulation. The 3-D optics aperture geometry is handled by a method of sub-gridscale placement of boundaries which explicitly includes the location of the optics wall in relation to the grid in the finite-difference form of Poisson's equation. Multiple apertures may be included explicitly in the simulation domain. Ion beam extraction from the discharge plasma is also included self-consistently. This 3-D particle simulation model is applied to analyze accel grid erosion. Grid erosion predicted by simulation is compared against erosion measurements taken during the long duration test of the NSTAR ion thruster. It is shown that the simulation not only predicts accurately all features in the erosion pattern observed experimentally but also gives excellent quantitative agreement with measured erosion depth.

Acknowledgement

We would like to acknowledge the assistance from R. Kafafy (Virginia Tech) in producing 3-D plots of the simulation results and M. Young (USC) in developing the 3-D DADI field solver. This work was carried out through support by the Jet Propulsion Laboratory, California Institute of Technology under a contract with NASA. Simulations are performed using the Cray supercomputer at JPL. Access to the JPL supercomputer was provided by funding from NASA Offices of Mission to Planet Earth, Aeronautics, and Space Science.

References

[1] Y. Arakawa and M. Nakano, An efficient three-dimensional optics code for ion thruster research, *AIAA 96-3198*, 1996.

[2] I. Boyd, D. VanGilder, and X. Liu, Monte Carlo simulation of neutral xenon flows in electric propulsion devices, *J. Propulsion and Power*, 14(6), 1998, pp1009.

[3] J. Douglass and J. Gunn, A general formulation of alternating direction methods, *Numerische Mathematik*, 6, 1964, pp428.

[4] S. Doss and K. Miller, Dynamic ADI methods for elliptic equations, *SIAM J. Numerical Analysis*, 16(5), 1979, pp837.

[5] D. Grote, Three-dimensional simulations of space-charge dominated heavy ion beams with applications to inertial fusion energy, Ph.D. thesis, University of California, Davis, 1994.

[6] D. Hewett, W. Larson, and S. Doss, Solution of simultaneous partial differential equations using dynamic ADI, *J. Comput. Phys.*, 101, 1992, pp11.

[7] M. Nakano and Y. Arakawa, Ion thruster lifetime estimation and modeling using computer simulation, *IEPC-99-145*, 1999.

[8] Y. Nakayama and P. Wilbur, Numerical simulation of ion beam optics for many-grid systems, *AIAA-2001-3782*, 2001.

[9] Y. Okawa and H. Takegahara, Particle simulation on ion beam extraction phenomena in an ion thruster, *IEPC 99-146*, 1999.

[10] X. Peng, W. Ruyten, V. Friedly, D. Keefer, and Q. Zhang, Particle simulation of ion optics and grid erosion for two-grid and three-grid systems, *Rev. Sci. Instrum.*, 65(5), 1994, pp1770.

[11] M. Tartz et al., Validation of a grid-erosion simulation by short-time erosion measurements, *IEPC 99-147*, 1999.

[12] Y. Muravlev and A. Shagayda, Numerical modeling of extraction systems in ion thrusters, *IEPC 99-162*, 1999.

[13] J. Polk, J. Anderson, J. Brophy, V. Rawlin, M. Patterson, J. Sovey, J. Hamley, An overview of the results from an 8200 hour wear test of the NSTAR ion thruster, *AIAA 99-2446*, 1999.

[14] S. Pullins, Y. Chiu, D. Levandier, and R. Dressler, Ion dynamics in Hall effect and ion thrusters: $Xe^{+}+Xe$ symmetric charge transfer, *AIAA 2000-0603*, 2000.

[15] J. Wang,D. Kondrashov, P. Liewer, and S. Karmesin, Three-dimensional deformable grid electromagnetic particle-in-cell for parallel computers, *J. Plasma Physics*, 61(3), 1999, pp367.

[16] J. Wang, D. Brinza, and M. Young, 3-D particle simulation modeling of ion propulsion plasma environment for Deep Space 1, *J. Spacecraft and Rockets*, 38(3), 2001, pp433.

[17] T. Westermann, Localization schemes in 2D boundary-fitted grids, *J. Computational Physics*, 101, 1992, pp307.

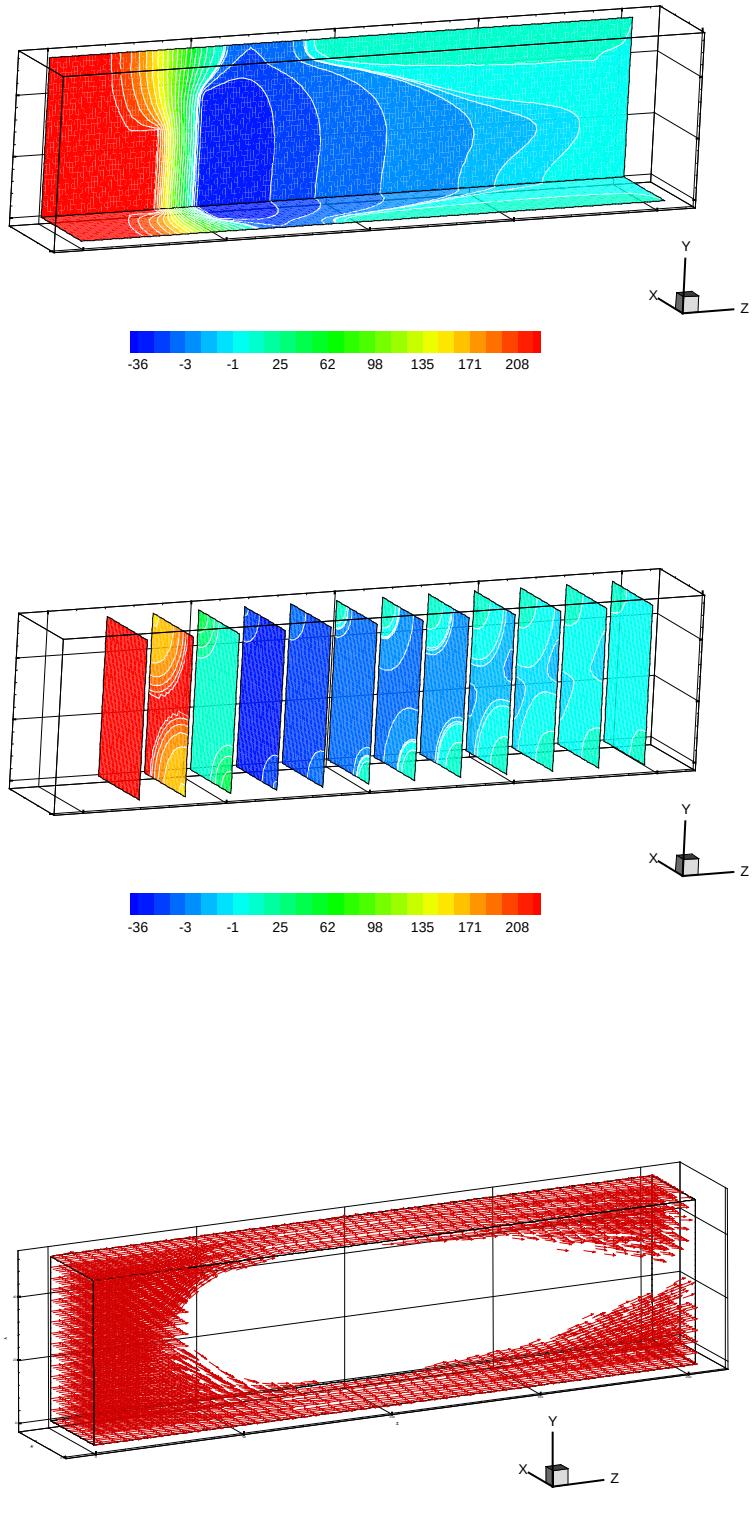

Figure 1: Potential contours and beam ion velocity directions. (The values of the potentials shown in the upper and middle panels are normalized by 5V.)

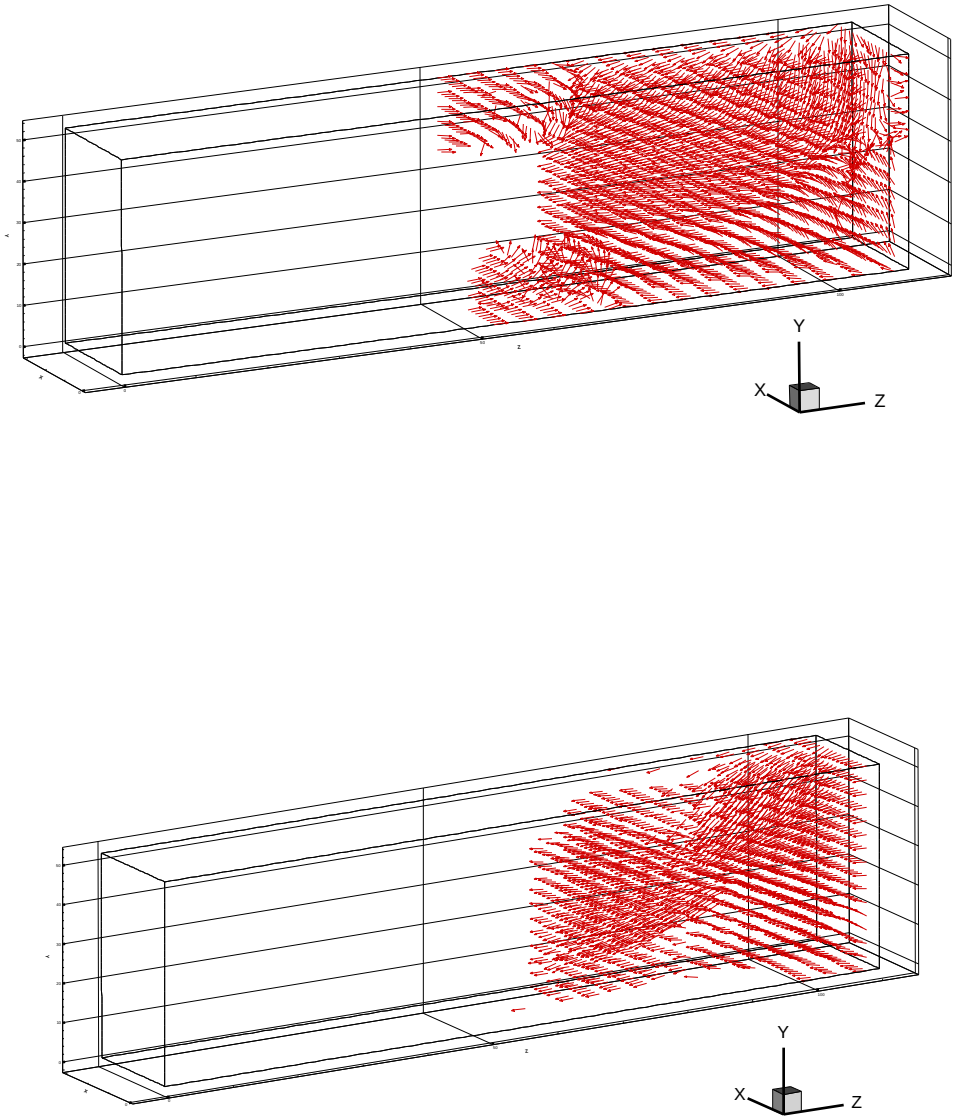

Figure 2: Velocity directions for charge exchange ions originated within 0.15cm of the accel grid (upper panel) and beyond 0.15cm downstream of the accel grid (lower panel)

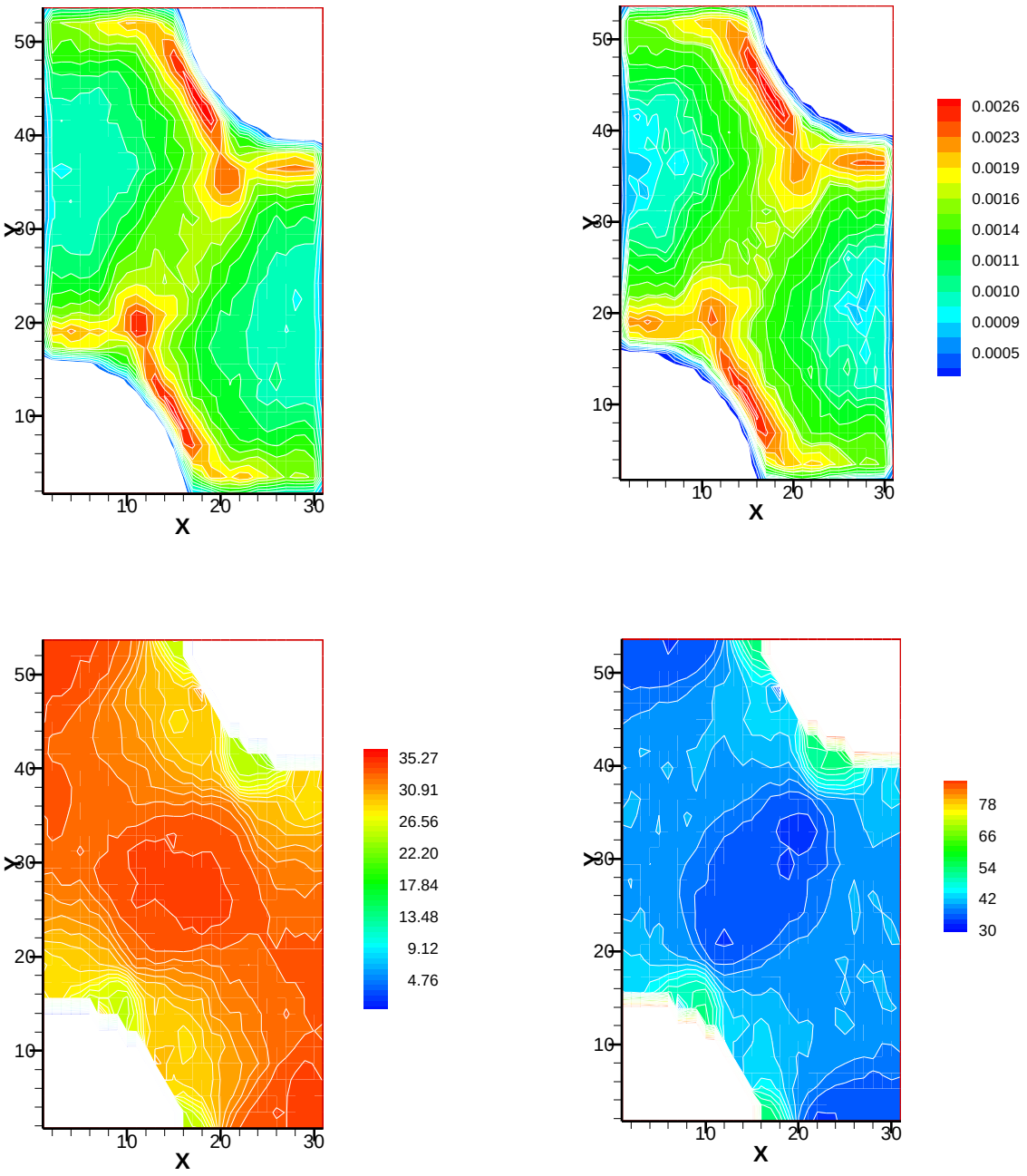

Figure 3: Accel grid impingement by charge exchange ions originated within 0.15cm of the accel grid: cincident urrent density (upper left), incident number flux (upper right), incident energy (bottom left), and incident angle (bottom right)

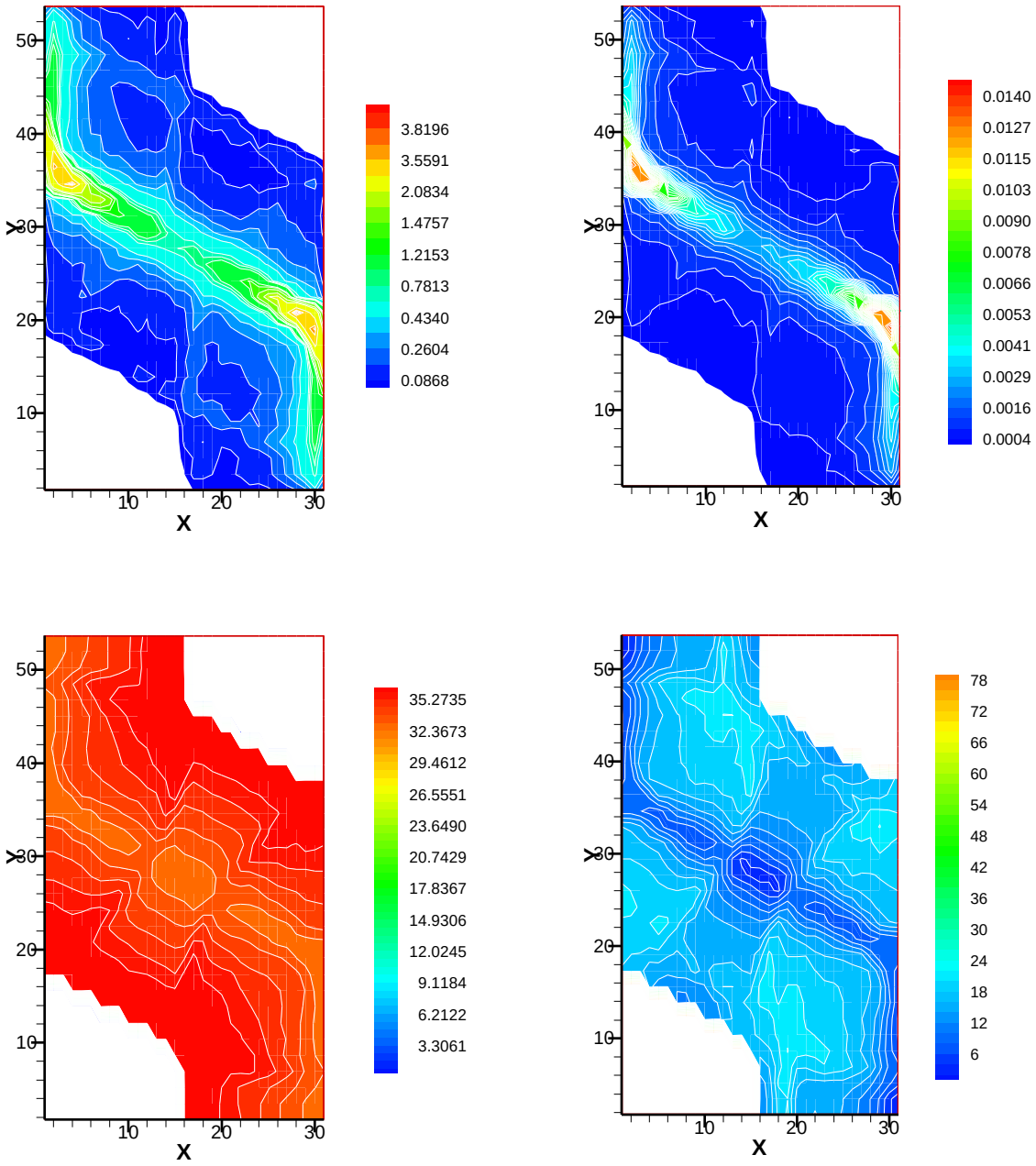

Figure 4: Accel grid impingement by charge exchange ions originated beyond 0.15cm downstream of the accel grid: cincident urrent density (upper left), incident number flux (upper right), incident energy (bottom left), and incident angle (bottom right)

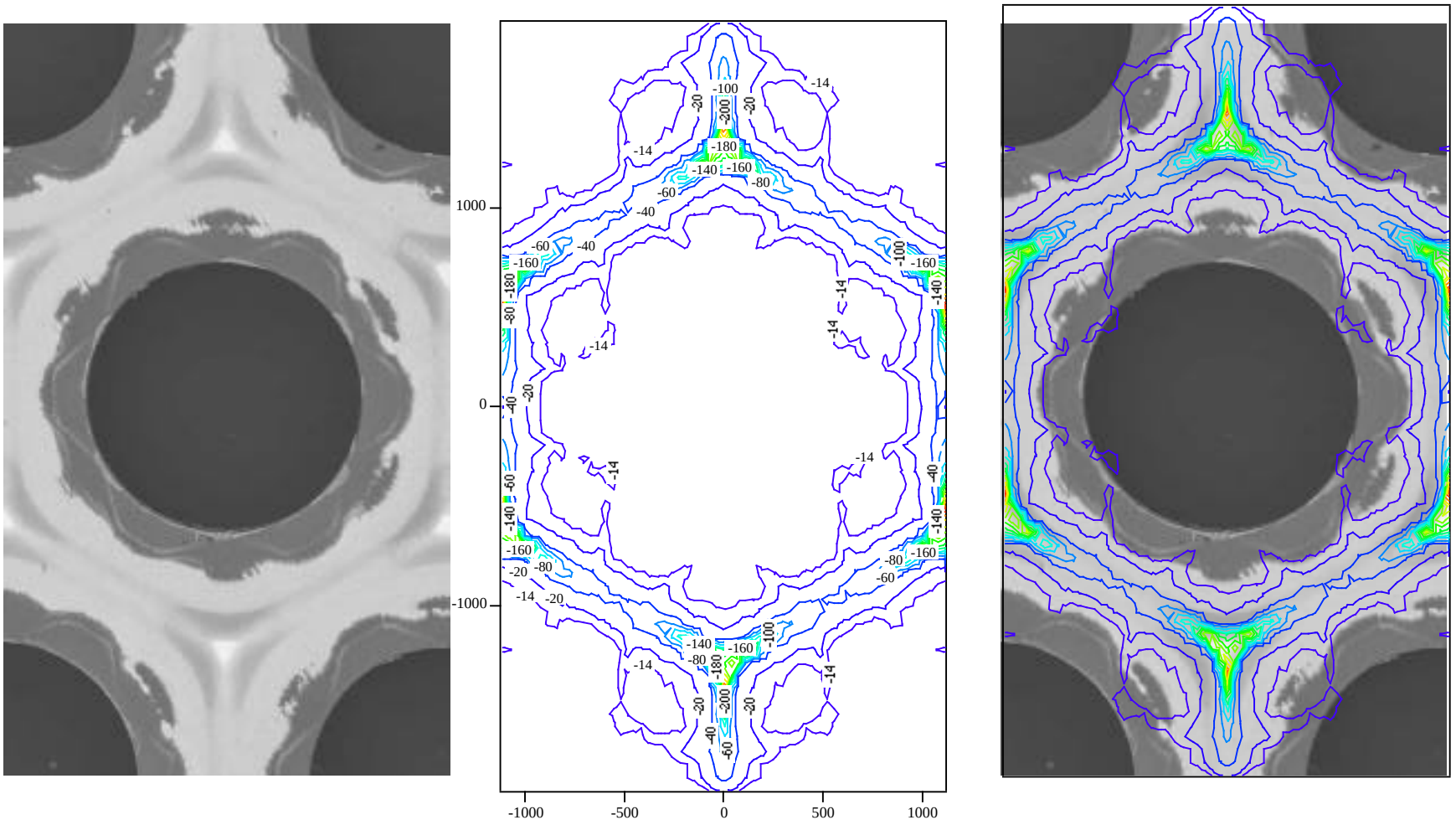

Figure 5: Comparison of simulation results with experimental data. Left: Photograph of erosion and deposition pattern after 8200 hours of operation. Middle: Simulation results for the same operating conditions; Right: Direct comparison of the erosion pattern.

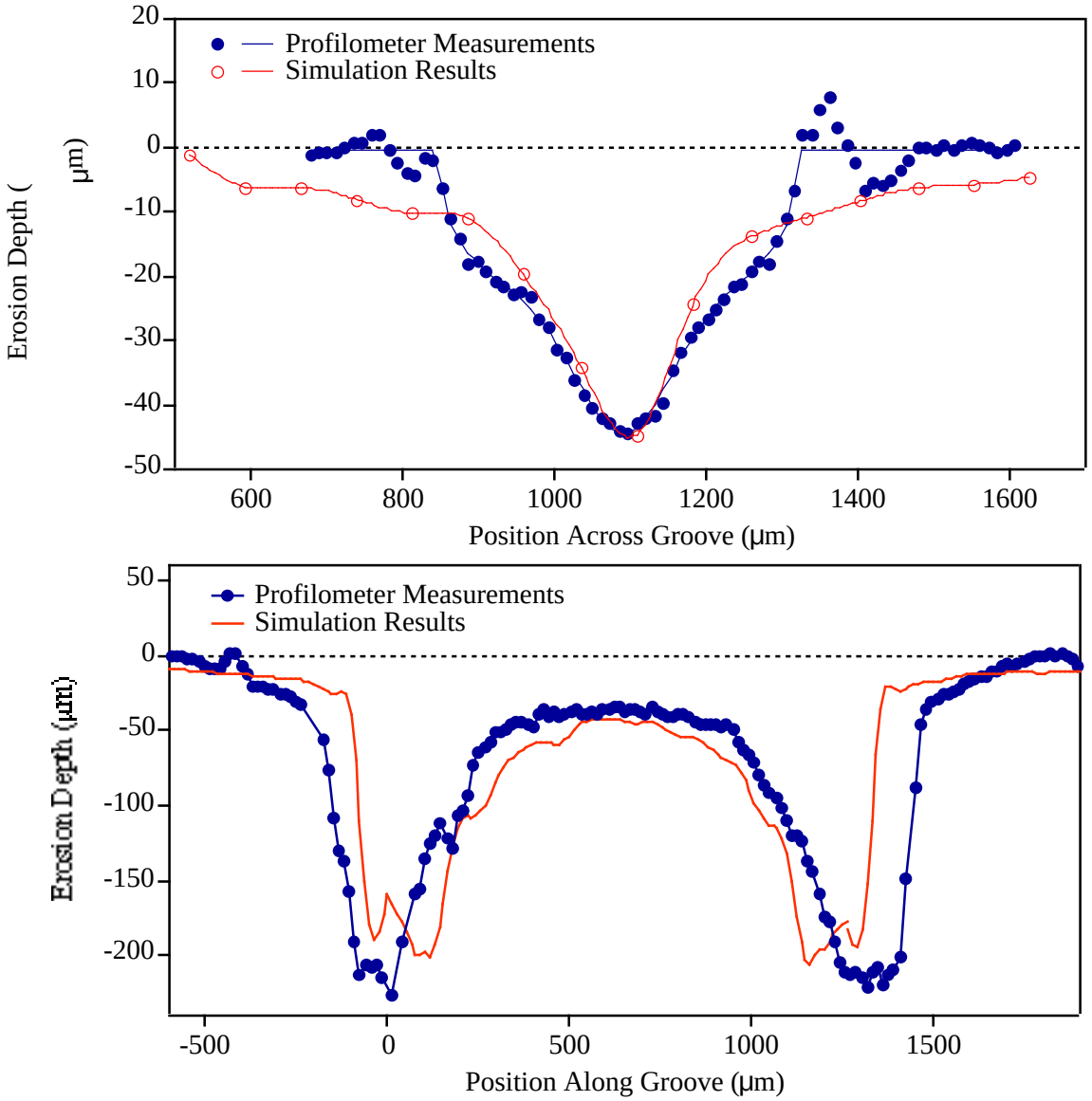

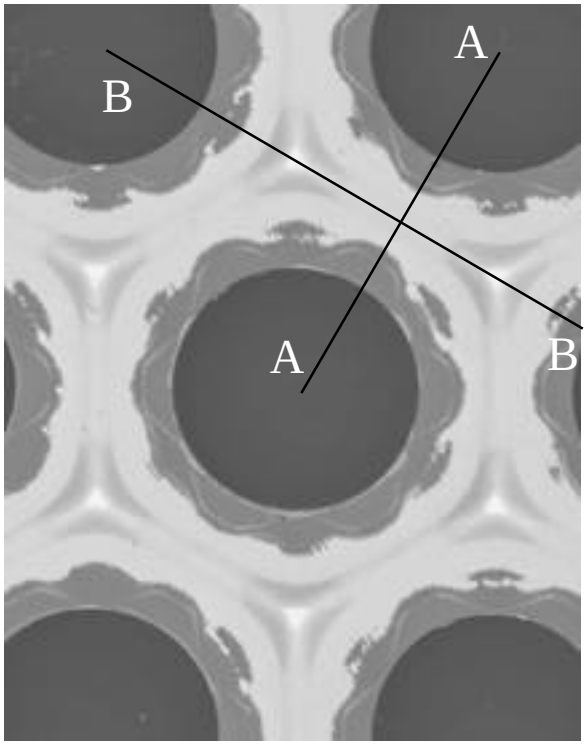

Figure 6: Comparison of simulation results with experimental data. Upper left: Erosion depth profile across groove (A-A). Bottom left: Erosion depth profile along the groove (B-B). Right: positions of the A-A and B-B profile on the grid.